ELSEVIER

Earth and Planetary Science Letters 125 (1994) 307–321

EPSL

Thermometrically inferred cooling rates from the Plattengneis, Koralm region, Eastern Alps

Karin Ehlers [a,*], Kurt Stüwe [b], Roger Powell [a], Mike Sandiford [b], Wolfgang Frank [c]

[a] *School of Earth Sciences, University of Melbourne, Parkville, Vict. 3052, Australia*
[b] *Department of Geology and Geophysics, The University of Adelaide, Adelaide, S.A. 5005, Australia*
[c] *Department of Geology, University of Vienna, A-1030 Vienna, Austria*

Received August 9, 1993; revision accepted April 12, 1994

Abstract

Closure of Fe–Mg exchange between garnet and biotite is used to estimate cooling rates from the Koralm region of the Austro-Alpine nappe complex east of the Tauern window in the Eastern Alps. Maximum cooling rates for a 700 m thick mylonitic shear zone, the Plattengneis, are at least an order of magnitude higher than those of surrounding country rocks. The cooling rate history inferred for the Plattengneis suggests exponentially decreasing cooling rates, whilst the cooling history of the surrounding country rocks is inferred to involve an approximately constant cooling rate. The fast cooling rates in the shear zone are interpreted as evidence for an additional energy input from an internal heat source, which may have been heat that was released during deformation, related to the Alpine nappe-stacking processes.

1. Introduction

That regional metamorphism proceeds as the natural conductive thermal response to crustal thickening has provided a unifying paradigm for metamorphic geology over the last decade and a half. This notion is founded on the classic work of the "Oxford" school [e.g., 1–3] which to some extent focusses on, and was inspired by, the geological evolution of the Tauern window in the Eastern Alps, where peak metamorphism apparently postdates the Late Cretaceous–early Tertiary Eoalpine convergent deformation by about 30 Ma. In view of the popularity of the paradigm it is, perhaps, surprising that not more attention has been paid to the fact that by far the greatest proportion of the Eastern Alpine crystalline rocks, particularly in the Austro-Alpine units, show no evidence of heating during the Tauern event [4,5].

The absence of the mid-Tertiary metamorphic overprint in the Eastern Alpine crystalline complex is generally interpreted as a consequence of it occupying a tectonically higher position than the Penninic rocks in the Tauern window. Indeed, the Gleimalm complex, adjacent to the Koralm complex, is interpreted as having reached

* Present address: Department of Earth Sciences, Monash University, Clayton, Melbourne, Vic. 3168, Australia.

SSDI 0012-821X(94)00078-D

the surface no later than about 60 Ma [6]. However, pressure estimates for the Eoalpine assemblages indicate that the depth of burial of the Koralm complex was comparable to that of the Penninic rocks in the Tauern window. Moreover, many of the interpretations of the exhumation history of the Koralm rest on the direct correlation of cooling with exhumation. Therefore, an important question to be resolved is the nature of cooling with exhumation. For example, cooling rates that are faster than those corresponding to geologically reasonable rates of exhumation may indicate cooling processes unrelated to exhumation. Also, the shape of the cooling rate evolution through time may bear significant information for the interpretation of the cooling process [7,8]. If it can be demonstrated that the Eoalpine cooling history is in part or completely unrelated to exhumation then this will have important implications for the interpretation of the Eoalpine thermal evolution of the Eastern Alps. For example, it allows the possibility that the Tertiary heating event in the Tauern window is not the natural conductive response to prolonged burial in that region of the Eastern Alps but that the Tauern and Eoalpine events are separated by a cooling phase.

One way to resolve these problems is via a study of the cooling history of the rocks. If rapid exhumation was responsible for the absence of the effect of the Tauern heating event, then the cooling history must be completed within a time frame that is short compared to the thermal time constant of the crust. If, on the other hand, cooling was the consequence of heating from an alternative process, then only cooling back to the stable geotherm may have been fast, whilst the completion of the cooling history during exhumation may be by an unrelated process. Moreover, erosion-terminated cooling histories will have increasingly faster cooling rates with decreasing temperature, whilst terranes heated by a transient heat source will have cooling rates which decrease with cooling. The cooling histories of the two scenarios are, therefore, likely to be qualitatively different. Cooling rates may be obtained from a number of techniques, including radiogenic dating and modelling of concentration profiles in minerals. Here, the Fe–Mg-exchange between garnet and biotite is used to determine the cooling rate evolution and establish the qualitative shape of the cooling history. It will be assumed that the growth and textural development of the garnet and biotite effectively ceased prior to cooling. Therefore the compositional changes in the minerals with cooling are dominated by diffusional exchange, and grain growth effects are minimal. A formalism for the relationship between closure temperature and cooling rate was first developed by Dodson [9,10] and extended to finite grain size parameters in [11]. We showed in [12] that the closure temperatures given by garnets of various sizes in a biotite matrix may be useful in determining changing cooling rates with cooling over a range of temperatures.

In this paper the Eoalpine thermal perturbation is explored by examining the cooling rate evolution of rocks in the vicinity of the Plattengneis, a major Eoalpine shear zone in the Koralm in Eastern Austria.

2. Tectonic setting

The Koralm unit is part of the Austro-Alpine basement complex, which enjoyed amphibolite to eclogite facies conditions in its deepest levels in the Cretaceous [13–15]. Deformation during and after this event resulted in the construction of a nappe pile in this region. According to Frank et al. [4] the nappe was emplaced from the southeast to the northwest, during which time a number of regionally important intracrustal shear zones were developed, including the Hirschegg and the Plattengneis. In its present position the Koralm unit forms the overturned lower limb of a nappe, the front of which is exposed at its northern boundary, where it overlies the somewhat lower grade Gleinalm unit. However, within the scale of our sampling, no grade change on a regional scale can be observed.

The Plattengneis forms the structurally highest unit of the Koralm basement unit. It is a mylonitic sheet up to 700 m thick, comprised predominantly of polymetamorphic pelitic meta-sedi-

ments (gneisses and micaschists), with interlayers of metacarbonates, pegmatites and metabasites (including eclogites) [16,17]. It dips about 5° to the southeast and its lineation trends N–S.

Microstructural analysis of rocks from the Koralm indicate a continuous decrease in strain rate from rocks in the Plattengneis to rocks in the footwall [18]. Rb/Sr and Sm/Nd dates for eclogite lenses within the sequence constrain the date of the eclogite event to within the range 150–90 Ma [13], whilst Rb–Sr and K–Ar dates on micas in the surrounding pelitic schist vary between 90 and 50 Ma [13,19–21]. The Cretaceous age of the eclogite lenses within the Plattengneis and the fact that they were subjected to the Plattengneis deformation means that the eclogite event was pre-deformational. The eclogite event reached pressures of 15 kbar and temperatures of 600–630°C [14,15]. The metasediments of the Plattengneis enclosing the eclogite lenses yield pressures and temperatures similar to those of the eclogites: 600–700°C and $P = 10–17$ kbar [17,22]. After this high-pressure event, intense deformation produced the Plattengneis. The youngest ages in this area, obtained from Rb–Sr and K–Ar on micas, yield Eoalpine ages of 60–57 Ma [13,19–21]. Thus, the Koralm crystalline complex did not experience the Tertiary, 30 Ma event, which may be observed in the Tauern window. In summary, for the purpose of this paper we use the Sm–Nd age of 90 Ma, representing a closure temperature of 650°C [23], as the age of the Plattengneis development, and the 60 Ma Rb–Sr age of biotite, representing a closure temperature of 500°C [24], for cooling through 500°C.

3. Samples and petrography

Samples from seven localities within the Plattengneis and three localities adjacent to it were studied (Fig. 1). Samples 48/92, 71/92, 72/92, 73/92, and 74/92 are from an approximately 15 km long, north–south traverse along the easternmost exposure of the Plattengneis and sample 26/92 comes from its westernmost exposure, near the Koralm summit. Samples 21/91, 24/92 and 28/92 are from the three localities outside the Plattengneis: sample 28/92 is from the hanging wall of the Plattengneis, near the Koralm summit, 28/92, 21/91 and 24/92 are from the footwall (Gaberl 21/91 and Krakaberg 24/92). The Krakaberg locality is close to the Plattengneis, whilst the Gaberl belongs to the northern part of the Koralm unit and is the locality furthest away from the Plattengneis. Whilst the latter three samples were, themselves, deformed as part of the pervasive Eoalpine deformation, they do not have a mylonitic fabric on a thin-section scale and we will refer to them henceforth as the 'undeformed' samples.

3.1. Plattengneis

Excellent structural and petrographic descriptions of the Plattengneis may be found in [16,17]. Modal mineral proportions (in volume percent) for the Plattengneis samples are very similar and are approximately: 5–10% garnet; 10–20% biotite; 20% muscovite; 0–7% kyanite; 50–60% quartz; 0.5–1% K-feldspar. Plagioclase occurs only as accessory components. The Plattengneis (samples 26/92, 48/92, 71/92, 72/92, 73/92 and 74/92) is a high-temperature mylonite which is characterized by alternating light and dark layers, each of which is about 0.5–1 mm in width. The light layers are characterised by *K-feldspar* augen with tails of fine-grained, dynamically recrystallized quartz. The dark layers consist predominately of quartz, biotite, muscovite, kyanite and garnet. *Quartz* forms ribbons or is recrystallised. *Kyanite* occurs in fine-grained aggregates, which form boudins parallel to the foliation. Biotite and muscovite follow, in general, the foliation and occur in two different grain sizes; as large grains 1–10 cm in size and small ones around 1–10 mm. *Muscovites* are Al- and Na-rich, with $X_{Al}^{M1} \approx 0.8$ and $X_{Na}^{A} \approx 0.015–0.035$. *Biotites* occur in pressure shadows of large garnet porphyroblasts and in boudins, together with small idiomorphic garnets. The modal abundances of garnet to biotite within these biotite–garnet boudins is about 1:5. Very little *plagioclase* is found in all samples; it only occurs as small, recrystallised grains.

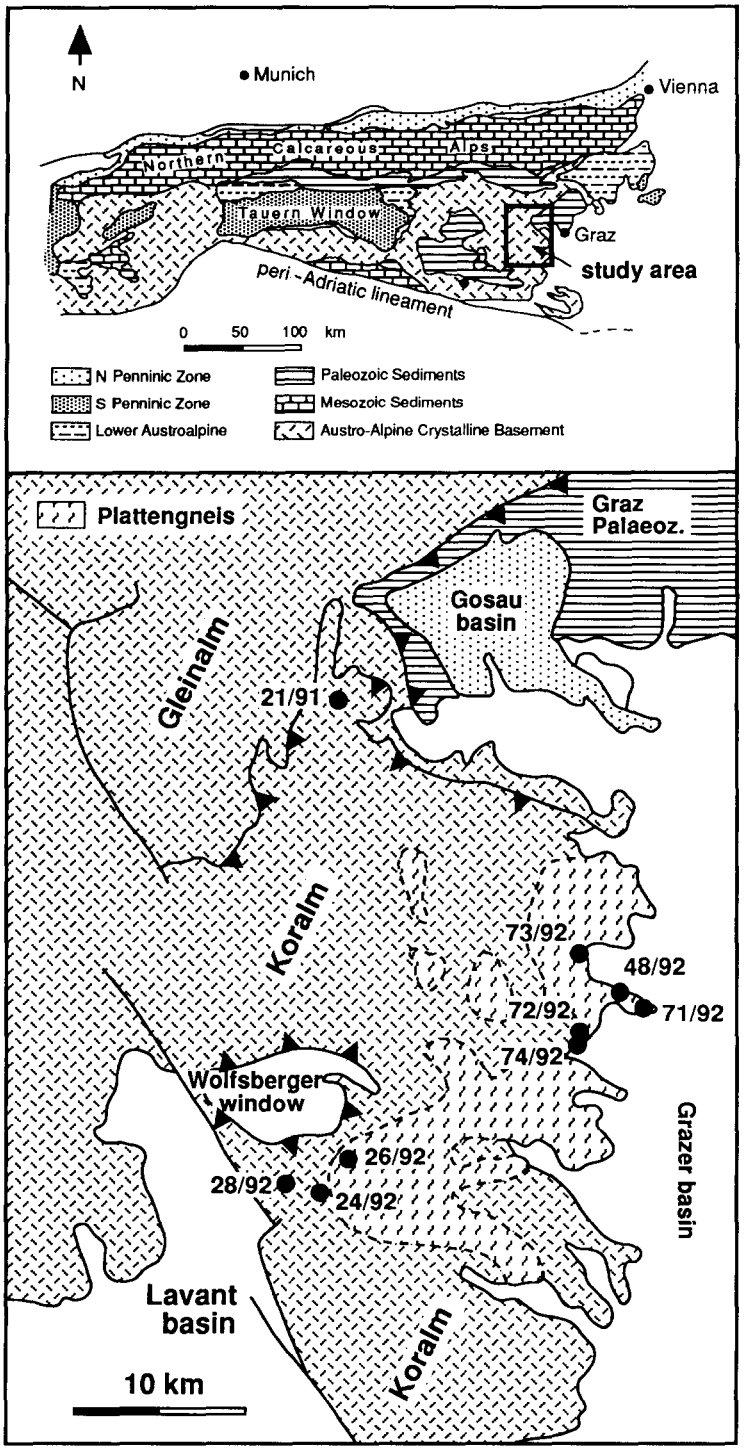

Fig. 1. Location of the Koralm complex [modified after Morauf, 19]. The dashed line indicates the approximate outline of the Plattengneis shear zone with schematically indicated foliation. The lobate outline of the shear zone is a consequence of its near surface-parallel dip on the eastern slope of the Koralm. The Koralm watershed runs approximately north–south through the sample location 26/92. The Lavant and Graz basins are Tertiary, the Gosau basin is Cretaceous. The sample localities in detail are: 26/92 = ridge between Seespitz and Hühnerstütze (near Koralm summit); 48/92 = Stainz; 71/92 = Stainz; 72/92 = Gams Quarry; 73/92 = Marhof Quarry; 74/92 = Säge Gams, outside Plattengneis; 21/91 = Buntschuhstraße, near Gaberl saddle; 24/92 = Krakaberg; 28/92 = Pontnig (half-way between Lavant valley and Krakaberg).

Two texturally and chemically distinct garnet types occur in all samples. *Garnet I* forms big porphyroblasts up to several centimetres in size, which are elongated parallel to the foliation and fractured perpendicular to it. Some of the garnet I grains show growth sectors, with a regular arrangement of solid inclusions of quartz and graphite. Garnet I often displays a rim of small, newly crystallised, idiomorphic garnet II. The typical average composition of garnet I is: 12–16% pyrope; 64–66% almandine; 3–5% grossular; and 11–19% spessartine. Garnet I grains always display prograde zoning patterns with increasing MgO and decreasing FeO and CaO from core to rim. Garnet I crystals, which are surrounded by biotite, show reversed zoning at their very rims, with decreasing MgO and increasing FeO from the core to the rim. Garnet I is interpreted as being pre-kinematic.

Garnet II is much smaller than garnet I, with grain sizes varying from a few microns to several millimetres. It is usually inclusion-free and is chemically quite distinct from garnet I, with 12–30% pyrope; 55–75% almandine; 1–20% grossular; 0–3% spessardine. Garnet II forms either idiomorphic crystals, overgrowing the deformational structures, or is deformed itself, typically showing elongated trails of garnet fragments in pressure shadows. These observations lead us to conclude that garnet II was syn- to post-kinematic. Larger garnet II grains (> 1 mm) display prograde zoning patterns (Fig. 2a), with increasing MgO and decreasing FeO and CaO from core to rim, with these patterns reversed at the very rims. The prograde zoning is interpreted as growth zoning; however, it is also possible that it is the product of diffusional equilibration during a period of temperature increase, of an older, pre-existing, garnet [25]. In any case, only the very rim displays reverse zoning, which is most likely the equilibration product of cooling. Small garnets (< 1 mm) show reversed zoning, with decreasing MgO and increasing FeO, which is interpreted as a cooling feature (Fig. 2b). The MnO content in retrograde-zoned garnets is generally low (MnO < 1.0 wt%) and CaO varies between the samples.

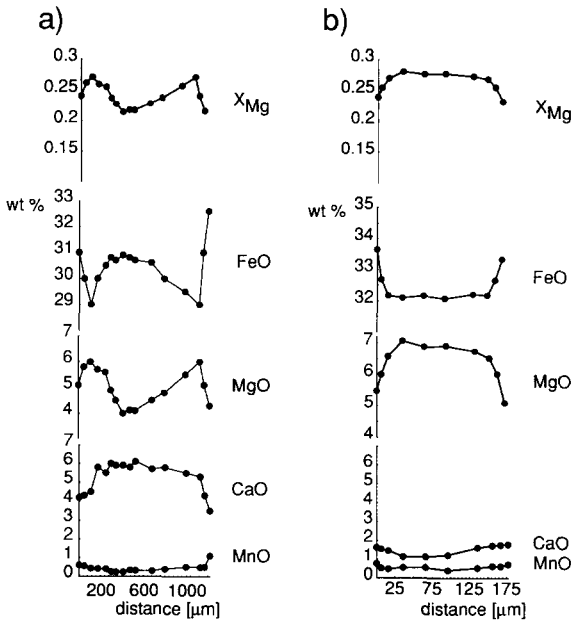

Fig. 2. (a) Concentration profile of a prograde-zoned garnet (corresponding to garnet I) with reversed rims. (b) A retrograde-zoned garnet corresponding to garnet II. Data for (a) are from [17]. Note the different scale for (a) and (b).

All the Plattengneis samples (48/92, 71/92, 72/92, 73/92 and 74/92) are very similar in their textures, mineral assemblages and mineral chemistry; only sample 26/92 differs from the other Plattengneis samples in that a higher proportion of micas (biotite and muscovite) overgrow the older foliation.

3.2. *'Undeformed' rocks*

All three 'undeformed' samples (21/91, 24/92 and 28/92) from outside the Plattengneis are weakly deformed with the same general tendency for garnet I to be pre-kinematic and garnet II and the micas to be syn- to post-kinematic. In contrast to the Plattengneis samples, a higher proportion of micas overgrow the old foliation. Modal mineral proportions (in volume percent) of all three samples are comparable and are approximately: 5–7% garnet; 15–25% biotite; 20–30% muscovite; 0–15% kyanite; 30–40% quartz. Some tex-

tural features are characteristic of the individual samples and are described below:

21/91: Large garnet II porphyroblasts, with pronounced sector zoning and rims of newly crystallised garnet II occur in a matrix of biotite–muscovite–quartz and a little K-feldspar. The micas follow the foliation and wrap around garnet porphyroblasts. Boudinaged layers of very fine-grained kyanite (few microns) alternate with boudinaged layers of quartz–muscovite. Biotites occur together with small garnet II crystals in boudins. The modal abundance of garnet to biotite within these biotite-rich layers is about 1:5 to 1:10. Some staurolite and occasional chlorite occur in this sample. Chlorite re-equilibrates with biotite and therefore alters the original biotite composition, which makes this sample difficult to use for closure temperature estimates. Thus, if it appears that biotite may have equilibrated with chlorite, then that biotite was not considered.

24/92: Abundant tourmaline occurs in biotite-rich layers, which define the foliation. Within these biotite-rich layers, biotite overgrows the older foliation. Most kyanite is replaced by fine-grained aggregates of muscovite. No large garnet I porphyroblasts were found; only garnet II is present throughout the sample.

28/92: White micas define the foliation and wrap around big garnet I crystals. Aggregates of small, idiomorphic garnet II occur, together with biotites. No kyanite occurs in this sample.

4. Closure temperature and cooling rate

All samples discussed in the last section contain garnet and biotite as the dominant Fe–Mg-bearing phases. The partitioning of Fe and Mg between these two phases is temperature dependent, forming the basis of a geothermometer [26]. However, the closure of Fe–Mg exchange is strongly dependent on cooling rate and grain size, which makes its use as a thermometer difficult at best. On the other hand, Fe–Mg exchange may be used to infer cooling rates. We begin with an outline of the underlying theory; for more details, see [12].

4.1. Theory

Let us assume that garnet is surrounded by abundant biotite, so that the volume proportion of garnet is small, and that the compositions of the garnet and biotite are homogenized at the peak metamorphic temperature. If Fe–Mg exchange between these phases is governed by volume diffusion during cooling, then Dodson's formalism [9,10] may be used to describe the relationship between closure temperature, cooling rate and grain size:

$$\frac{Q}{RT'_c(y)} = \ln\frac{D_0}{l'^2}(1-y^2)\frac{RT'_c(y)^2}{Q_s} + G(y) \quad (1)$$

[12, eq. (3)], where $T'_c(y)$ = the closure temperature for the centre of a garnet cut at position, y (with $y = 0$ referring to a cut through the centre of the grain and $y = 1$ to a cut through the rim); s = the cooling rate; D_0 = the pre-exponential factor of garnet in the Arrhenius equation; Q = the activation energy of garnet; R = the gas constant; l' = the observed half-width of garnet; and $G(y)$ = the closure function. The actual half-width of the garnet, l, is related to the observed half-width, l', by $l' = l\sqrt{1-y^2}$. $G(y)$ depends on the geometry of the grains and the position y within the grain [10, table 2]. This equation applies to a wide range of cooling histories [11,27]. Dodson, who derived Eq. (1) for geochronological systems, suggested that it would also apply to petrological systems. This has been confirmed using numerical diffusion experiments by Ehlers and Powell [11, see also 28]. An example of the applicability of Eq. (1) to petrological systems may be found in relation to Spear's fig. 5b [28]. Numerical runs for this figure were carried out for a small garnet to biotite ratio of 0.001 and therefore meet Dodson's boundary conditions. Consequently, fig. 5b of Spear [28] may be exactly reproduced by applying Eq. (1), using the same diffusion data [of 30] and $G(y = 0) = 1.96$ (for spherical geometry).

In petrological systems such as garnet–biotite, an independent estimate of closure temperature is available by applying a geothermometer equation involving the diffusion components. Then, if the diffusion data are known, Eq. (1) may be used

to calculate cooling rates by rearranging Eq. (1) so that:

$$s(y) = \frac{D_0}{l'^2}(1-y^2)\frac{RT_c'(y)}{Q} \times \exp\left(-\frac{Q}{RT_c'(y)} + G(y)\right) \quad (2)$$

[12, eq. 5], with the cooling rate, $s(y)$, depending on the section position, y. It is important to note that $T_c'(y)$ and Q occur in the exponential term, which means that a small error in $T_c'(y)$ or Q will yield a large error in $s(y)$. However, if the one set of diffusion data and the one geothermometer are used, they will shift all the results, as discussed in a later section. A cooling rate given by Eq. (2) depends on knowledge of the position of section y within the garnet. However, in thin section this position is usually unknown. Closure temperature, $T_c'(0)$, and cooling rate, $s(0)$, obtained from the observed centre of garnet, assuming the grain is cut through its centre ($y = 0$), will underestimate the actual closure temperature and cooling rate. Thus, if the actual position of section is y, the corresponding closure temperature, $T_c'(y)$, and cooling rate, $s(y)$, are higher than $T_c'(0)$ and $s(0)$, defining a locus on a $\ln s(y)$–$T_c'(y)$ diagram (Fig. 3). In Fig. 3, the black dot corresponds to the calculated apparent $T_c'(0)$ and $s(0)$, with $l = l'$, as though the garnet is cut through its centre, so that $y = 0$. However, if the actual garnet is much bigger and the garnet is cut through its edge, so that $y = 0.9$, for example, then the centre of the actual garnet (which is not observed) would yield a much higher closure temperature and cooling rate than the one calculated as though $y = 0$ (Fig. 3, grey dot, for example).

For the thermometer equation used above and the diffusion data of [30], the locus from $T_c'(0)$ and $s(0)$ in $T_c'(y)$–$\ln s(y)$ space is observed to be given by the equation:

$$\ln s(y) = \ln s(0) + (T_c'(y) - T_c'(0)) \times \left(-0.00113 + \frac{11300}{T_c'(0)^2}\right) \quad (3)$$

in which $s(y)$ and $T_c'(y)$ correspond to a particular section position [12]. If many garnet–biotite pairs are analysed then the actual cooling rate history must intersect all loci, at least within a 95% likelihood, on a $\ln s(y)$–$T_c'(y)$ diagram. This was examined and verified using Monte Carlo simulations in [12].

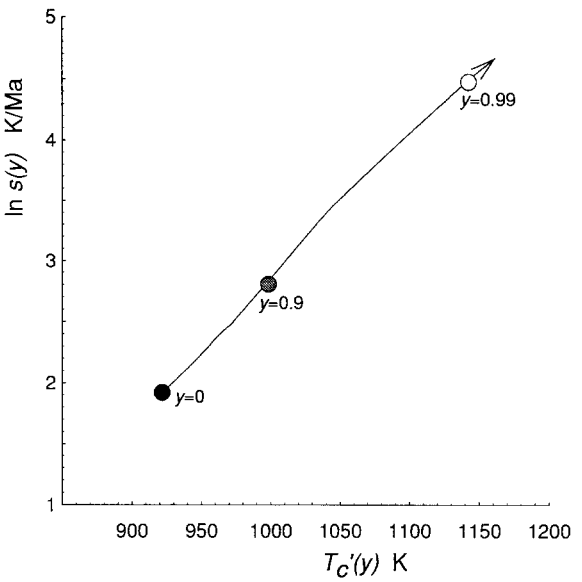

Fig. 3. The calculated $T_c'(0)$ and $s(0)$ for one garnet–biotite pair (●) and its locus. If the observed garnet (●) is cut through its centre then the calculated $T_c'(0)$ and $s(0)$ coincide with the actual closure temperature, $T_c(0)$, and cooling rate, s. If, however, the actual garnet is much bigger than the apparent one, so that the observed garnet size is, for example, a section at $y = 0.9$ of a big garnet (that is, close to its edge), then the actual $T_c(0)$ and s of the centre of the bigger garnet (which cannot be observed) will be much higher than the observed one (grey dot, for example).

In order to apply this method to the Koralm, we used analyses of observed core compositions of garnets and biotites, with the thermometer expression derived using the data of Holland and Powell [29] for Fe–Mg exchange between garnet and biotite, to give the closure temperature assuming the grain is cut through its centre (i.e. $y = 0$):

$$T_c'(0) = \frac{44.97}{0.01456 + 3R \ln K_D} \quad (4)$$

with:

$$K_D = \frac{(1 - X_{Mg}^{g})}{X_{Mg}^{g}} \frac{X_{Mg}^{bi}}{(1 - X_{Mg}^{bi})}$$

The apparent cooling rate, $s(0)$, was calculated using the experimentally determined Mg self-diffusion coefficients for garnet with $Q = 239$ kJ/mol and $D_0 = 9.81 \times 10^{-9}$ m^2/s [30] and $G(0) = 1.96$ for the spherical case [10, table 2]. Taking these values for D_0, Q and $G(0)$ and transforming Eq. (2) into units of K/Ma, Eq. (2) for $y = 0$ becomes:

$$s(0) = 10.7478\left(\frac{T_c'(0)}{l'}\right)^2 \exp\left(-\frac{28784}{T_c'(0)} + 1.96\right) \quad (5)$$

Apparent half-widths (l') of garnets were measured from the probe sections. It is important to note that the cooling rate obtained from Eqs. (2) and (5) using the geothermometrically determined closure temperature is the cooling rate at the closure temperature. This means that centres of big garnets, closing at higher temperatures, give the cooling rate at higher temperatures; the centres of smaller garnets give the cooling rate at lower temperatures. It follows that rocks with a wide range of garnet grain size, such as a mylonite (for example the Plattengneis), are likely to cover a large part of the cooling rate history.

4.2. Application to the Koralm rocks

Within the Koralm rocks, prograde-zoned garnets occur next to retrograde-zoned garnets. Garnet I is always prograde-zoned, but garnet II may be prograde- or retrograde-zoned, depending on its grain size. Only retrograde-zoned garnet II may be used, due to the requirement for using Dodson's formalism that the garnet should have equilibrated at the peak temperature. Traditionally, garnet I is believed to be of pre-Alpine age, whilst garnet II is Eoalpine. However, without absolute ages for these garnets, the presence of prograde and retrograde zoning suggest that garnet II also formed pre-Alpine but the time at temperature during the Eoalpine was sufficient to homogenize the smaller grains totally. Regardless of when they formed, smaller garnets equilibrated at peak metamorphic conditions in the Eoalpine. As it is critical to use only retrograde-zoned garnets which are surrounded by abundant biotite the following procedure was applied. (Note that only garnet II within the biotite boudins or layers were used for the cooling rate calculations).

Firstly, the approximate grain size of garnets which allows re-equilibration during cooling for geologically reasonable cooling rates must be established. This may be done either by using Eq. (1) to calculate the grain size, cooling rate and closure temperature dependency, or fig. 5b of Spear [28] may be used and corresponding grain sizes may be read off directly. From that, it may be seen that only the smallest garnets (< 1 mm) could have re-equilibrated during cooling for a cooling rate range of 0.1–3000 K/Ma. Accordingly, an initial selection of garnet–biotite pairs, which was done under the optical microscope, focused on small (< 1 mm), inclusion-free garnets. An additional requirement for selecting garnets was that they were surrounded by abundant biotite.

Quantitative mineral analyses were carried out with a CAMECA automated three-spectrometer electron microprobe at the University of Melbourne. The wavelength-dispersive method was used with an accelerating potential of 15 kV and a sample current of 30 nA. The standard errors for each element are likely to be $\approx 1\%$ relative. Biotites were analysed using a 6 μ beam size, whilst garnets were analysed with a 1 μ beam.

An initial microprobe examination confirmed that only the smallest garnets display retrograde zoning. The challenge now was to distinguish between large garnets (> 1 mm), which may have prograde zoning preserved and are cut near their edge, and truly small grains (< 1 mm). This was done by obtaining three analyses: one from the apparent centre and two from the opposing rims. If it was found that X^g_{Mg} at the rims was higher than at the centre, indicating prograde zoning, then these garnets were discarded for further analysis. If, however, the rims had lower X^g_{Mg} than the centre, then these garnets were examined further, which involved microprobe traverses through the apparent centre of the garnet. Such traverses included 5–20 analyses, depending on the size of the garnet (Fig. 2b, for example). On average, 3–5 garnets of the same apparent grain size needed to be analysed to find the desired

retrograde-zoned one. If a garnet was choosen, then the surrounding biotites were analysed. This involved the analysis of biotites adjacent to the garnet (~ 5–10 μm from the garnet rim) and biotite analyses successively further away. Only if all biotites, which are believed to belong to the equilibrium volume of the garnet, displayed homogeneous composition would this particular garnet–biotite pair be accepted. The biotite analyses were averaged.

The accepted garnet–biotite pairs (Table 1) were then used to calculate the apparent closure temperatures, using Eq. (4), and apparent cooling rates, using Eq. (5). As an example, take the garnet–biotite pair 72/6 (Table 1): $X^{g}_{Mg} = 0.263$ and $X^{bi}_{Mg} = 0.626$. Substituting into Eq. (4) yields a $T'_c(0)$ of 845 K. Taking this $T'_c(0)$ and the apparent radius of the garnet, $l' = 0.0000338$ m (Tables 1, 2b), and substituting into Eq. (5) yields an apparent cooling rate of $s(0) = 82$ K/Ma (ln $s(0) = 4.4$ K/Ma). Substituting these $T'_c(0)$ and $s(0)$ values into Eq. (3) and assuming a temperature, $T'_c(y)$, of 950 K, at the start of cooling, Eq. (3) gives a $s(y)$ of 360 K/Ma (ln $s(0) = 5.9$ K/Ma). Thus, a line may be drawn from the $T'_c(0)$ of 845 and ln $s(0)$ of 4.4 to $T'_c(y) = 950$ K and ln $s(y) = 5.9$. This line defines the locus in $T'_c(y)$–ln $s(y)$ space for the garnet–biotite pair of sample 72/6.

Table 1
Selected garnet–biotite analyses ($X_{Mg} = Mg/(Mg+Fe)$)

	72/6-g	72/6-bi	73/10-g	73/10-bi	28/6-g	28/6-bi
l' [m]	0.0000338		0.000016		0.00007	
SiO_2	37.96	37.22	37.51	36.02	38.31	36.84
TiO_2	0.04	3.26	0.13	3.79	0	2.53
Al_2O_3	21.53	17.54	21.46	17.31	22.88	19.58
Cr_2O_3	0	0.01	0.03	0	0	0
FeO	31.92	13.90	27.05	14.86	34.99	18.20
MnO	0.57	0.01	0.47	0.06	0.31	0
MgO	6.38	13.05	5.14	11.90	3.85	9.45
CaO	1.56	0.03	7.63	0.05	0.72	0.01
Na_2O	-	0.07	-	0.08	-	0.08
K_2O	-	9.74	-	9.39	-	8.164
Total	99.96	94.83	99.42	93.46	101.06	94.85
cation						
Si	2.988	5.538	2.959	5.476	3.003	5.519
Ti	0.002	0.365	0.008	0.434	0	0.285
Al	1.998	3.075	1.995	3.103	2.100	3.457
Cr	0	0.002	0.002	0	0	0
Fe	2.101	1.73	1.785	1.889	2.292	2.279
Mn	0.038	0.0.001	0.032	0.007	0.02	0
Mg	0.749	2.895	0.605	2.696	0.45	2.108
Ca	0.132	0.005	0.645	0.008	0.06	0.001
Na	-	0.021	-	0.025	-	0.030
K	-	1.849	-	1.821	-	1.56
X_{Mg}	0.263	0.626	0.253	0.588	0.164	0.48

5. Results

The garnet and biotite analyses, available on request from the first author, give $T'_c(0)$ using Eq. (4), and the corresponding $s(0)$ from Eq. (5); they are shown in Fig. 4a for the Plattengneis, and Fig. 4b for the adjacent undeformed rocks. All results are listed in Tables 2 and 3. These $T'_c(0)$ and $s(0)$ values underestimate the actual $T_c(0)$ and s values by the amount that relates to the distance between the actual and the apparent grain centre. Lines in Fig. 4 mark the locus of $T'_c(0)$ and $s(0)$ if the actual grain centre is assumed to be progressively further away from the apparent grain centre. These lines are calculated with Eq. (3) and are cut off at 973 K, a temperature near the assumed peak temperature of the Plattengneis. Cooling histories were obtained by fitting a line on the ln $s(y)$–$T'_c(y)$ diagrams (shaded areas, Fig. 4), which intersects all loci, at least with 95% likelihood. Garnet–biotite pairs of the Plattengneis rocks define a very steep cooling history in a ln $s(y)$–$T'_c(y)$ diagram (Fig. 4a), whilst garnet–biotite pairs of the undeformed rocks suggest a more or less constant cooling history. However, because only few suitable garnet–biotite pairs could be obtained for the undeformed rocks, it is possible that more data for the undeformed rocks may point towards a higher cooling rate. On the other hand, from a statistical viewpoint, the dataset of the undeformed rocks may be representative.

Results indicate that closure temperatures for the same garnet size are on average 50–100°C higher for the Plattengneis than the undeformed samples. Cooling rates of the Plattengneis are 100–3000°C/Ma in the temperature range of 580–700°C, and 1–100°C/Ma in the temperature range of 400–580°C (Fig. 4a). The cooling rate of the undeformed rocks is 1–30°C/Ma for a temperature range of 400–600°C (Fig. 4b). These cooling rate changes with temperature may be used to establish large parts of the T–t history. However, before discussing the temperature history, sources of uncertainties in the analysis need to be discussed, starting with the influence of Ca and Mn in garnet on closure temperature.

Garnets from the Plattengneis have higher py-

rope contents than undeformed samples (Fig. 5a), as expected from the calculated closure temperatures. There is a general tendency for the garnets of the Plattengneis to have somewhat higher Ca contents than the garnets of undeformed rocks. Some samples of the undeformed rocks are higher in Mn. However, most importantly there is *no* correlation between the Ca and/or Mn content and the calculated closure temperatures (Fig. 6). It should be pointed out that the thermometer expression used here assumes ideal mixing in garnet and in biotite and does not consider non-ideality, for example with respect to the grossular and/or spessartine components in garnet. In or-

Table 2
$T_c'(0)$ and $s(0)$ for all garnets from the Plattengneis
(a)

no	loc	X^g_{Mg}	X^{bi}_{Mg}	ℓ' [cm]	$T_c'(0)$ K	ln $s(0)$
3	26	0.1782	0.5501	0.003	779.3	1.5
4	26	0.1993	0.5501	0.004	828.7	3.3
6	26	0.1662	0.5501	0.00185	752.0	1.1
7	26	0.2471	0.5501	0.0105	949.4	6.1
8	26	0.1739	0.5501	0.0017	769.5	2.2
9	26	0.2482	0.5501	0.012	952.4	5.9
10	26	0.2517	0.5501	0.0103	961.9	6.5
11	26	0.1688	0.5501	0.00165	757.9	1.6
12	26	0.165	0.5501	0.00235	749.2	0.5
13	26	0.1437	0.5501	0.00065	701.6	0.3
14	26	0.1858	0.5501	0.00435	796.9	1.7
15	26	0.1697	0.5501	0.0014	759.9	2.1
16	26	0.1782	0.5501	0.0013	779.3	3.2
17	26	0.1735	0.5501	0.00145	768.6	2.5
1	48	0.262	0.621	0.003	853.2	4.9
2	48	0.257	0.62	0.0017	844.5	5.7
3	48	0.266	0.62	0.002	863.3	6.2
4	48	0.263	0.6117	0.004	871.5	5.1
5	48	0.227	0.62	0.001	784.3	4.0
6	48	0.172	0.574	0.001	734.8	1.4
7	48	0.143	0.574	0.00025	674.6	0.5
1	48	0.3184	0.67	0.004	878.2	5.4
2	48	0.2994	0.67	0.0015	841.7	5.8
3	48	0.2648	0.67	0.0065	779.4	0.009
4	48	0.2777	0.67	0.00455	802.1	1.8
5	48	0.246	0.67	0.00125	747.5	1.6
6	48	0.2736	0.67	0.00345	794.8	2.0
7	48	0.2667	0.68	0.002	767.5	1.8
8	48	0.2511	0.68	0.00175	741.9	0.7
9	48	0.2491	0.68	0.00125	738.6	1.2
10	48	0.2637	0.68	0.002	762.5	1.5
1	71	0.2679	0.6387	0.00235	835.2	4.6
2	71	0.2897	0.6387	0.00604	879.3	4.6
3	71	0.2743	0.6387	0.00459	847.9	3.9
6	71	0.2826	0.64	0.0019	862.3	6.2
7	71	0.2523	0.6328	0.00283	814.2	3.3
8	71	0.257	0.6328	0.00255	823.4	4.0
9	71	0.2744	0.6328	0.004	858.4	4.6
10	71	0.2705	0.643	0.0025	833.0	4.4
11	71	0.2846	0.6426	0.00496	861.7	4.3
13	71	0.2816	0.6462	0.00542	849.4	3.6
14	71	0.2885	0.6462	0.00556	863.1	4.1
15a	71	0.2794	0.64	0.00366	855.9	4.6
16	71	0.2965	0.6311	0.0022	908.4	7.7
17	71	0.2882	0.6311	0.0026	890.4	6.7
18	71	0.2834	0.65	0.00926	846.3	2.4
15b	71	0.2794	0.6486	0.00834	840.9	2.5

(b)

no	loc	X^g_{Mg}	X^{bi}_{Mg}	ℓ' [cm]	$T_c'(0)$ K	ln $s(0)$
1a	72	0.2753	0.6417	0.00785	844.7	2.6
2	72	0.2772	0.6417	0.00991	848.5	2.3
3	72	0.2516	0.6326	0.00299	813.1	3.2
4	72	0.2693	0.6326	0.00435	848.3	4.0
5a	72	0.2672	0.6326	0.00325	844.1	4.4
6a	72	0.2628	0.626	0.00338	846.3	4.4
7	72	0.2594	0.626	0.0029	839.4	4.4
8	72	0.2816	0.64	0.00834	860.3	3.2
9	72	0.2448	0.64	0.00175	788.8	3.1
10	72	0.2354	0.64	0.0013	771.4	2.8
12	72	0.2833	0.6625	0.0061	824.6	2.3
13	72	0.265	0.6371	0.00868	832.1	1.9
14	72	0.259	0.6371	0.0032	820.4	3.4
17	72	0.2627	0.6549	0.00473	799.0	1.6
18	72	0.2575	0.6549	0.0013	789.6	3.7
19	72	0.2814	0.6456	0.0048	850.0	3.9
20	72	0.2671	0.6748	0.00235	776.1	1.9
1b	72	0.289	0.6443	0.01	867.6	3.1
5b	72	0.286	0.644	0.0198	862.2	1.5
6b	72	0.283	0.644	0.00473	856.0	4.1
6a	73	0.2687	0.6054	0.00225	895.6	7.2
7a	73	0.2637	0.6054	0.00555	884.4	5.0
8	73	0.2483	0.592	0.00245	873.6	6.2
9a	73	0.2686	0.6091	0.00215	888.6	7.0
10a	73	0.253	0.588	0.0016	891.6	7.7
6b	73	0.266	0.597	0.0015	905.2	8.4
7b	73	0.276	0.6005	0.007	921.9	5.9
9b	73	0.207	0.61	0.00393	759.4	0.01
1	74	0.2756	0.6594	0.0019	815.5	4.2
2	74	0.2731	0.6594	0.0023	810.9	3.6
3	74	0.2874	0.6393	0.00625	873.5	4.3
4	74	0.2299	0.6393	0.0018	762.3	1.7
5	74	0.2443	0.6393	0.0034	788.9	1.8
6	74	0.2532	0.6445	0.00235	797.6	2.9
7	74	0.2995	0.64	0.00909	897.5	4.5
8	74	0.2959	0.6319	0.00344	905.5	6.7
9	74	0.305	0.6271	0.0024	935.5	8.5
10	74	0.2488	0.621	0.00145	826.1	5.2

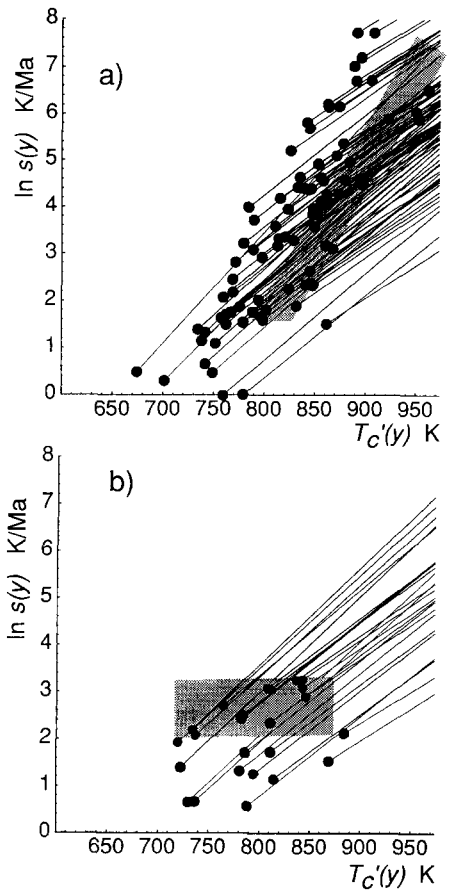

Fig. 4. ln $s(y)$–$T_c'(y)$ diagrams (a) for the Plattengneis and (b) for the undeformed samples. • = observed $T_c'(0)$ and $s(0)$ values; solid lines = loci of $T_c'(y)$ and ln $s(y)$ for section positions in the same crystal closer to its potential centre, if the section position is not known. These lines move away from the measured apparent $T_c'(0)$ and $s(0)$ and were calculated using Eq. (3). The inferred actual cooling history must intersect all loci, at least within error (shaded areas).

der to minimize the possible influence of these elements on $T_c'(0)$, only garnets with less than 10% grossular and less than 2% spessartine have been used. However, the general trend of higher cooling rates and closure temperatures within the Plattengneis in comparison to adjacent rocks does not change even if grains with larger concentrations of these additional components are considered. Thus, we believe that the resulting $T_c'(0)$–ln $s(0)$ relationship is not a compositional artifact related to the grossular or spessartine components. Therefore, all analyses, regardless of the Ca or Mn content were used.

Considering the sources of uncertainty, it is convenient to distinguish between systematic and random errors. Systematic errors will tend to shift the set of loci in the $T_c'(y)$–ln $s(y)$ diagram as a whole, without much changing the relative loci positions. Random errors will affect individual results and shift loci relative to each other. Whilst systematic errors may not change the overall conclusions of the derived cooling histories, random errors may potentially have a dramatic influence on the analysis. Systematic errors arise from the uncertainties in the diffusion data of garnet (activation energy, Q, and pre-exponential factor, D_0) and the geothermometer equation. As an example of a systematic error, the effect of diffusion data (Q, D_0) on the results is shown on Fig. 7. It may be seen that, depending on the choice of diffusion data, all results are shifted systematically to lower or higher cooling rates, respectively. Given the nature of Eq. (1), the error on individual data may be as big as 4 log units (Fig. 7). However, more importantly, this systematic

Table 3
$T_c'(0)$ and $s(0)$ for all garnets from the undeformed rocks

no	loc	X_{Mg}^{g}	X_{Mg}^{bi}	ℓ' [cm]	$T_c'(0)$ K	ln $s(0)$
1	21	0.157	0.49	0.00425	810.5	2.4
5	21	0.141	0.52	0.00125	729.7	0.7
6	21	0.137	0.52	0.0005	719.9	1.9
7	21	0.138	0.52	0.0007	722.4	1.4
1	24	0.1239	0.4408	0.00205	783.3	2.5
2	24	0.1327	0.4408	0.00301	811.0	3.1
3	24	0.1407	0.4408	0.00485	836.5	3.3
4	24	0.108	0.4408	0.00065	733.7	2.2
5	24	0.1316	0.4408	0.00275	807.5	3.1
6	24	0.109	0.4408	0.00075	736.8	2.1
7	24	0.1179	0.4408	0.00115	764.5	2.7
9	24	0.1359	0.4637	0.00605	788.0	0.6
10	24	0.1437	0.4637	0.00585	811.1	1.7
11	24	0.1448	0.4637	0.0084	814.2	1.2
12	24	0.1295	0.4554	0.00345	780.4	1.3
13	24	0.1147	0.4554	0.0015	736.3	0.7
14	24	0.13	0.4554	0.00205	782.0	2.4
1	28	0.163	0.48	0.0055	842.6	3.3
2	28	0.143	0.48	0.00325	785.8	1.7
3	28	0.177	0.48	0.0225	883.6	2.1
4	28	0.196	0.52	0.0225	868.8	1.5
6	28	0.164	0.48	0.007	845.5	2.9
7	28	0.146	0.48	0.005	794.2	1.3
8	28	0.163	0.48	0.006	842.6	3.1

shift of the data hardly affects the shape of the cooling history and, as such, the general trend of fast cooling rates within the Plattengneis and the much slower ones in the undeformed rocks.

As discussed above the calculated $T_c'(0)$ values from Eq. (4) do not involve a Ca and Mn correction, because at least within the data, there is no evidence for a systematic effect of Ca/Mn on $T_c'(0)$ (Fig. 6). A list of sources of random errors may be found in [12]. The most important ones relate to compositional differences between garnet–biotite pairs and mis-identification of geometric relations between garnet and biotite. Random errors are likely to be much less than the systematic ones and they are unlikely to contribute uncertainties of more than 1 log unit in s.

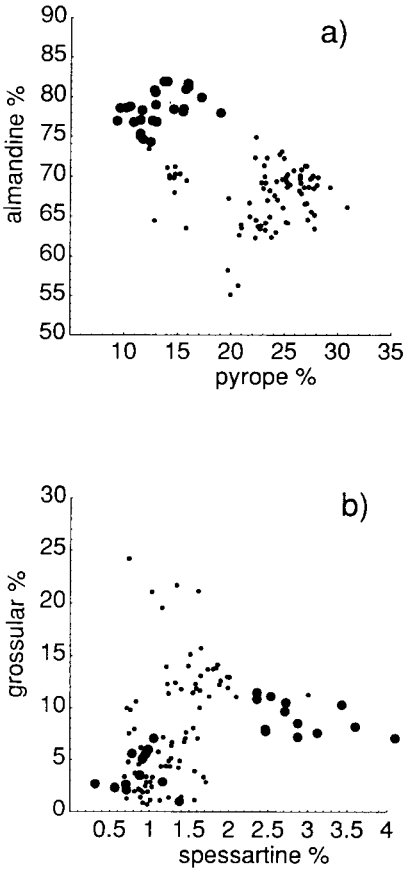

Fig. 5. (a) Pyrope and almandine components of all garnets used for cooling rate estimates. (b) Grossular and spessartine components for the same garnets. Big dots are for undeformed samples, small dots are from the Plattengneis.

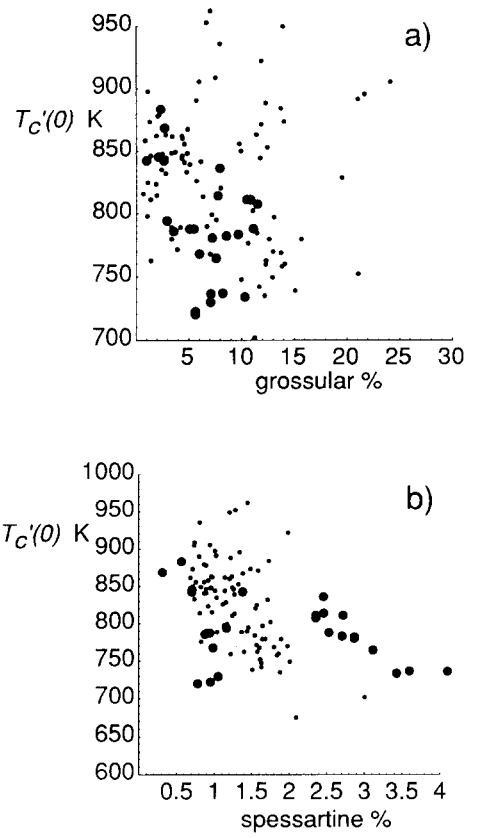

Fig. 6. (a) $T_c'(0)$ versus grossular and (b) $T_c'(0)$ versus spessartine. The wide scatter indicates that there is no dependency of $T_c'(0)$ on the grossular or spessartine contents. Symbols as in Fig. 5.

We can now interpret the results, in particular how T–t relationships are deduced from the $T_c'(y)$–ln $s(y)$ relationships. We begin with the interpretation of the Plattengneis.

5.1. The derivation of the T–t histories

The cooling rate trend for the Plattengneis is shown in Fig. 4a. Given the likely uncertainties (see above) one cooling rate band can be assigned to the data, noting that the band should cut each line, at least within error. A line within this band used below is $s = e^{-0.0355T+27.2}$. The cooling rate trend for the undeformed rocks is shown in Fig. 4b, showing that closure temperatures are, on average, 50–100°C lower than those of the Plattengneis and the corresponding cooling rates are

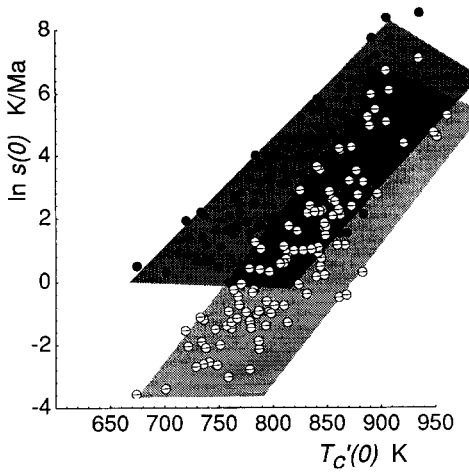

Fig. 7. The influence of different sets of diffusion data on the results. ● = calculated using diffusion data of Cygan and Lasaga [30] ($D = 9.81 \times 10^{-9}$ exp(239/RT)m^2/s); ○ = calculated with the diffusion data of Lasaga et al. [31] ($D = 2.75 \times 10^{-6}$ exp(292.6/RT) m^2/s). All data, Plattengneis and undeformed rocks, are plotted.

at least an order of magnitude lower at the same temperature. Within likely error, a constant cooling rate of ln $s = 2.5 \pm 0.5$°C/Ma is consistent with the data.

The cooling rate histories (Fig. 8a) may be transformed into histories by integration. The resulting T–t history of the Plattengneis is:

$$t = \frac{e^{27.2}}{0.0355}\left(e^{-0.0355T_0} - e^{-0.0355T}\right) + t_0$$

and for the undeformed rocks is:

$$t = \frac{1}{12.2}(T - T_0) + t_0$$

(Fig. 8b), where T_0 = the temperature of the rocks at time t_0, for example in the Plattengneis the time and temperature of the start of exponential cooling after the metamorphic peak. These T–t histories may be fixed in absolute time only with independent geochronological information. Using the geochronological constraints discussed earlier, the path should pass through 90 Ma at 650°C, and 60 Ma at 500°C (dots in Fig. 8b).

6. Tectonic implications

The cooling history inferred from Fig. 8b implies a transient heating process causing fast cooling rates at high temperatures early in the history of the Plattengneis and much slower cooling rates after the transient event. However, whilst we are confident about the interpretation of the transient event, the relative position in the T–t space of the undeformed rocks is based on the interpretation of one geochronological age constraint.

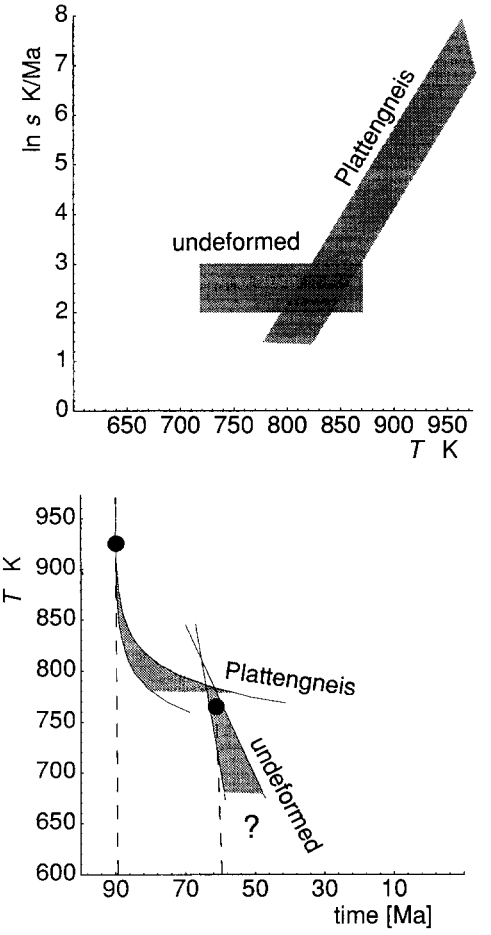

Fig. 8. (a) ln s–T_c diagram showing the cooling rate histories for the Plattengneis and the undeformed samples from Fig. 4. (b) T–t histories derived from the T_c–s histories. ● = Sm/Nd ages for garnet at 90 Ma and the Rb/Sr age of biotites of 60 Ma. Shaded area indicates one possible T–t path for the Koralm rocks.

Additionally, it must be pointed out that below 450°C the garnet–biotite system is closed and therefore the T–t history is not known. Additional qualitative evidence for the transience of this heating event is that only the smallest garnets (< 1 mm) have re-equilibrated, even though they were heated to ≈ 973 K. Many of these small garnets in the Plattengneis may be recrystallisation products from during or after the deformation. All larger garnets still preserve growth zoning but were mostly broken up during the deformation. A short transient heating event is also supported by other independent evidence related to the age dating of the eclogites. Sm/Nd and Rb/Sr isochrons for an eclogite sample give exactly the same age of 95.5 ± 9.5, whilst Sm/Nd on garnet and white mica in the surrounding metapelites gives 91 ± 4 [13]. This suggests a short time interval between the eclogite metamorphism and the closure of the Sm/Nd system in garnet and white mica. One possibility for such a transient heating event is shear heating related to the formation of the Plattengneis.

This interpretation suggests that care should be taken with the direct inference of the exhumation history from geochronology in the Austro-Alpine. For example, the two geochronological age constraints used for Fig. 8b will yield a constant cooling history after the eclogite metamorphism of 5°C/Ma, if fitted with a straight line. In fact, we suggest that it may not be unrealistic for cooling of the Koralm complex to have occurred largely isobarically; that is, cooling at depth without exhumation.

Acknowledgement

We would like to thank Ingeborg Ehlers, Ulla Stüwe and Lilo Wallner for sampling the Plattengneis in wintery Austria, and F. Spear and two anonymous reviewers for critical reviews. ARC supported this research.

References

[1] M.J. Bickle, C.J. Hawkesworth, P.C. England and D. Athey, A preliminary thermal model for regional metamorphism in the Eastern Alps, Earth Planet. Sci. Lett. 26, 13–28, 1975.

[2] S.W. Richardson and R. Powell, Thermal causes of the Dalradian metamorphism in the Central Highlands of Scotland, Scott. J. Geol. 12, 237–268, 1976.

[3] P.C. England and S.W. Richardson, The influence of erosion upon the mineral facies of rocks from different metamorphic environments, J. Geol. Soc. London 134, 210–213, 1977.

[4] W. Frank, M. Esterlus, I. Frey, G. Jung, A. Krohe and J. Weber, Die Entwicklunggeschichte von Stub- und Koralpenkristallin und die Beziehung zum Grazer Paläozoikum, Hochschulschwerpunkt 15, 263–293, 1983.

[5] H.W. Flügel and P. Faupel, Geodynamics of the Eastern Alps, Franz Deuticke, 1987.

[6] F. Neubauer, R.D. Dallmeyer, I. Dunkel and D. Schrink, Late Cretaceous cooling of the metamorphic Gleinalm dome, Eastern Alps, in a sinistral wrench corridor: Kinematics, cooling history and sedimentary response, Terra Nova Abst. Suppl. 2, 1–48, 1992.

[7] K. Stüwe, K. Ehlers, M. Sandiford and R. Powell, Cooling histories of metamorphic terrains. A simple parameterisation with implications for distinguishing orogenic histories, J. Geophys. Res., submitted.

[8] D.K. Holm and R.K. Dokka, Interpretation and tectonic implications of cooling histories: An example from the Black Mountains, Death Valley extended terrane, California, Earth Planet. Sci. Lett. 116, 63–80, 1993.

[9] M.H. Dodson, Closure temperature in cooling geochronological and petrological systems, Contrib. Mineral. Petrol. 40, 259–274, 1973.

[10] M.H. Dodson, Closure temperature in cooling systems, Mater. Sci. Forum 7, 145–154, 1986.

[11] K. Ehlers and R. Powell, An empirical modification of Dodson's equation for closure temperature in binary systems, Geochim. Cosmochim. Acta 58, 241–248, 1994.

[12] K. Ehlers, R. Powell and K. Stüwe, Cooling rate histories from garnet–biotite equilibrium, Am. Mineral., in press.

[13] M. Thöni and E. Jagoutz, Some new aspects of dating eclogites in orogenic belts: Sm–Nd, Rb–Sr, and Pb–Pb isotopic results from the Austroalpine Saualpe and Koralpe type-locality (Carinthia/Styria, southeastern Austria), Geochim. Cosmochim. Acta 56, 347–368, 1992.

[14] Ch. Miller, Petrology of the type locality eclogites from the Koralm and Saualpe (Eastern Alps), Austria, Schweiz. Mineral. Petrol. Mitt. 70, 287–300, 1990.

[15] Ch. Miller, H.G. Stosch and St. Hoernes, Geochemistry and origin of eclogites from the type locality Koralm and Saualpe, Eastern Alps, Austria, Chem. Geol. 67, 103–118, 1988.

[16] A. Krohe, Kinematics of Cretaceous nappe tectonics in the Austroalpine basement of the Koralpe region (eastern Austria), Tectonophysics 136, 171–196, 1987.

[17] I. Wimmer-Frey, Gefüge- und Metamorphoseuntersuchungen am Plattengneis der Zentralen Koralm, W-Steiermark, Ph.D. Thesis, Univ. Vienna, 1984.

[18] T. Flöttmann, G. Kleinschmidt and D. Wolf, Deformationanalyse der unteren Gneisgruppe in der südlichen Koralpe (Ostalpen), Carinthia II, 179–202, 1986.
[19] W. Morauf, Die permische Differentation und die alpidische Metamorphose des Granitgneises von Wolfberg, Koralpe, SE-Ostalpen, mit Rb/Sr- und K/Ar-Isotopenbestimmungen, Tschermarks Petrogr. Mitt. 27, 169–185, 1980.
[20] W. Morauf, Rb-Sr- und K-Ar-Isotopenalter an Pegmatiten aus Kor- und Saualpe, SE-Ostalpen, Österreich, Tschermarks Mineral. Petrogr. Mitt. 28, 113–129, 1981.
[21] W. Morauf, Rb–Sr- und K–Ar Evidenz für eine intensive alpidische Beeinflussung der Paragesteine in Kor- and Saualpe. SE-Ostalpen, Österreich, Tschermarks Mineral Petrogr. Mitt. 29, 255–282, 1982.
[22] K. Stüwe and R. Powell, *PT* paths from modal proportions. Application to the Koralm complex, Eastern Alps, Contrib. Mineral. Petrol, in press.
[23] K. Mezger, E.J. Essene and A.N. Halliday, Closure temperatures of the Sm–Nd system in metamorphic garnets, Earth Planet. Sci. Lett. 113, 397–409, 1992.
[24] R.A. Cliff, Isotopic dating in metamorphic belts, J. Geol. Soc. London 142, 97–110, 1985.
[25] S. Chakraborty and J. Ganguly, Compositional zoning and cation diffusion in garnets, in Advances in Physical Geochemistry, Vol. 8, J. Ganguly, ed. pp. 121–175, Springer, Berlin, 1990.
[26] J.M. Ferry and F.S. Spear, Experimental calibration of the partitioning of Fe and Mg between biotite and garnet, Contrib. Mineral. Petrol. 66, 113–117, 1978.
[27] O.M. Lovera, F.M. Richter and T.M. Harrison, The $^{40}Ar/^{39}Ar$ thermochronometer for slowly cooled samples having a distribution of diffusion domain sizes, J. Geophys. Res. 94, 17917–17935, 1989.
[28] F.S. Spear, On the interpretation of peak metamorphic temperatures in light of garnet diffusion during cooling, J. Metamorph. Geol. 9, 379–388, 1991.
[29] T.J.B. Holland and R. Powell, An enlarged and updated internally consistent thermodynamic dataset with uncertainties and correlations: the systems K_2O–Na_2O–CaO–MgO–MnO–FeO–Fe_2O_3–Al_2O_3–SiO_2–C–H_2–O_2. J. Metamorph. Geol. 8, 89–124, 1990.
[30] R.T. Cygan and A.C. Lasaga, Self-diffusion of magnesium in garnet at 750°C to 900°C, Am. J. Sci. 285, 328–350, 1985.
[31] A.C. Lasaga, S.M. Richardson and H.D. Holland, The mathematics of cation diffusion and exchange between silicate minerals during retrograde metamorphism, in Energetics of Geological Processes, S.K. Saxena and S. Bhattachanji, eds., pp. 353–388, Springer, Berlin, 1977.